CHEMISTRY OF MATERIALS

Communication

pubs.acs.org/cm

Synthesis of Hierarchical Graphdiyne-Based Architecture for Efficient Solar Steam Generation

Xin Gao,[†,§] Huaying Ren,[†,‡,§] Jingyuan Zhou,[†,‡] Ran Du,[†] Chen Yin,[†,‡] Rong Liu,[†,‡] Hailin Peng,[†] Lianming Tong,[*,†] Zhongfan Liu,[*,†] and Jin Zhang[*,†]

[†]Center for Nanochemistry, Beijing Science and Engineering Center for Nanocarbons, Beijing National Laboratory for Molecular Sciences (BNLMS), College of Chemistry and Molecular Engineering, Peking University, Beijing 100871, People's Republic of China

[‡]Academy for Advanced Interdisciplinary Studies, Peking University, Beijing 100871, People's Republic of China

Supporting Information

Efficient solar steam generation plays an important role in various energy-related applications including water desalination,[1−3] environmental remediation,[4] and large-scale solar-thermal power plant.[5] Photothermal materials absorb light and convert it to heat through thermalization and nonradiative recombination of photoexcited electron−hole pairs, and offer a promising solution for solar steam generation with high efficiency. Several factors need to be considered for the improvement of the solar steam generation effeciency: broadband absorption to utilize the full solar spectrum, localization of the thermal energy at the evaporative surface to minimize heat loss from the bulk water, and multiple channels for continuous water provision and vapor flow. For example, Ti_2O_3 nanoparticles have been reported as a photoabsorber material for efficient solar steam generation owing to its narrow bandgap corresponding to absorption in almost the full solar spectrum.[6] A self-floating film based on Au nanoparticles was designed for enhanced solar steam generation, where most of the thermal energy was utilized to heat up the water only at the evaporative surface.[7] Recently, carbon-based materials with inherently broad absorption bandwidth have emerged as new candidates for efficient solar steam genetation, such as carbon-based foam[8] and graphene oxide-based materials.[9−11] However, they hardly exhibited well-controlled nano- and microstructures that are critical for light trapping and vapor flow, limiting the further improvement of photothermal efficiency. Therefore, the development of photothermal materials with both broadband absorption and well-defined micro/nanostructures is of great importance in the field of solar steam generation.

Graphdiyne (GDY),[12] with highly π-conjugated structure of sp- and sp^2-hybridized carbons, has recently appeared as a new allotropic form of carbon nanomaterials, and has been applied in Li ion battery,[13,14] photoelectric devices,[15−17] catalysis,[18,19] and environmental remediation.[20] On the other hand, its narrow band gap (0.46 eV)[21] endows its remarkable potential for solar steam generation with an optical absorption window extending to ∼2700 nm. Unlike graphene and other nanocarbons typically acquired by using harsh condition such as high-temperature CVD growth,[22] GDY is often obtained from bottom-up syntehsis via wet chemical method, facilitating a much more flexible control of structures. For example, previously we have successfully fabricated vertical GDY nanosheets on diverse substrates.[17] Herein, a new structure based on three-dimensional (3D) copper foam supported one-dimensional (1D) CuO nanowires anchoring with vertical two-dimensional (2D) GDY nanosheets was developed. In this architecture, the copper foam provides the self-supporting sketelon, CuO nanowires are responsible for most solar absorption, and GDY nanosheets could simultaneously trap the light via structual factors (by increasing the light traveling distance inside materials) and enhance the light absorption through its intrinsic narrow band gap. As a result, a photothermal conversion efficiency of up to 91% has been achieved, making this GDY-based structure promising not only for efficient solar steam generation but also in diverse fields such as water desalination and environmental remediation.

The fabrication process of GDY-based hierarchical architecture is illustrated in Figure 1a. First, a film of $Cu(OH)_2$ nanowires was synthesized on a copper foam via the surface oxidation reaction.[23] The formation of $Cu(OH)_2$ nanowires was visually observed by the color change of the copper foam from light-yellow to light-blue (Figure S1). Scanning electron microscopy (SEM) images (Figure S2) show that the skeleton of the copper foam was uniformly covered by vertically grown, hair-like nanowires with diameters in the range of 100−500 nm

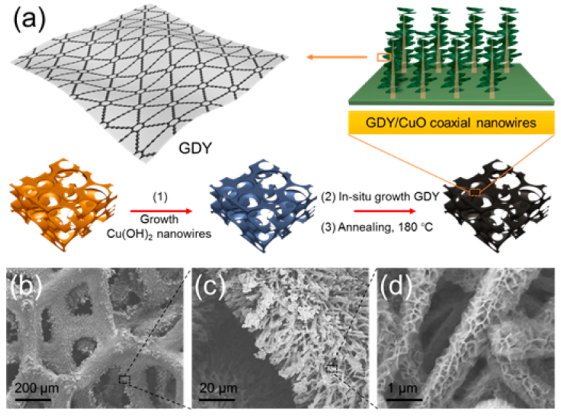

Figure 1. (a) Schematic illustration of GDY-based hierarchical architecture. SEM images of the copper foam coated by GDY/CuO coaxial nanowires (b−d).

Received: May 4, 2017
Revised: June 27, 2017
Published: June 27, 2017

DOI: 10.1021/acs.chemmater.7b01838
Chem. Mater. 2017, 29, 5777−5781

and lengths in the range of 10−25 μm. Subsequently, vertical GDY nanosheets were in situ synthesized on the surfaces of $Cu(OH)_2$ nanowires via Glaser−Hay coupling reaction (detailed description, see SI).[24] In this way, 1D $Cu(OH)_2$ nanowires were uniformly wrapped by a honeycomb-like structure consisted of vertical 2D GDY nanosheets. Finally, the as-prepared sample was annealed at 180 °C for 2 h for complete dehydration. The X-rays diffraction (XRD) pattern of as-prepared nanowires on copper foam (Figure 2c) could be assigned to the monoclinic CuO phase (JCPDS No. 48-1548),[25] confirming the formation of CuO on the copper foam substrate. As a result, a hierarchical architecture with GDY/CuO coaxial nanowires (Figure S3) was obtained on the porous copper foam, providing both channels for vapor flow (Figure 1b) and well-controlled nano- and microstructures for efficient solar absorption (Figure 1c,d).

The structure and elementary composition of the GDY-based nanowires foam were further studied. As shown by the transmission electron microscopy (TEM) image in Figure 2a,

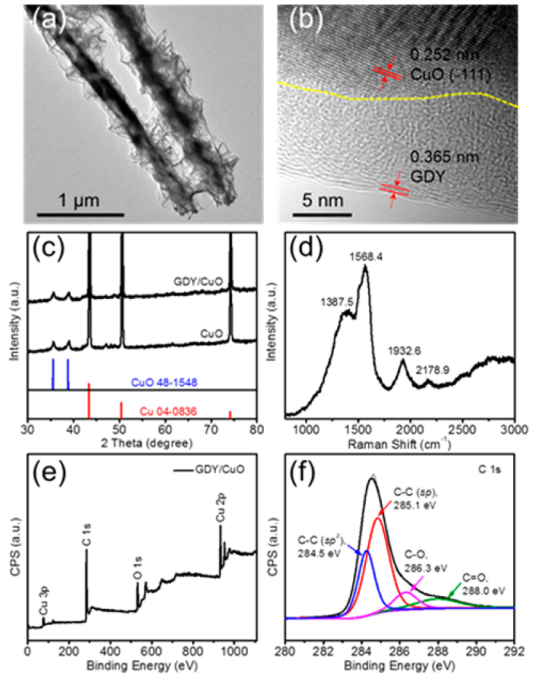

Figure 2. (a) TEM image of GDY/CuO nanowires. (b) HRTEM image of the GDY/CuO interface. (c) XRD patterns of CuO and GDY/CuO nanowires film on copper foam. (d) Typical Raman spectrum of GDY nanowalls grown on nanowires. (e) XPS spectrum of GDY/CuO coaxial nanowires. (f) Corresponding high-resolution core level XPS spectrum of C 1s.

CuO nanowires were uniformly wrapped by the GDY nanosheets. High-resolution TEM (HRTEM) image of the GDY/CuO interface is shown in Figure 2b. A fringe spacing of 0.252 nm was clearly observed, consistent with the (−111) lattice planes of CuO.[26] In addition, the fringe spacing of 0.365 nm corresponds to the layer-to-layer distance of GDY nanosheets.[27] To confirm further the formation of the core−shell nanowire structure, a high-angle annular dark field-scanning transmission electron microscopy (HAADF-STEM) image of a GDY/CuO coaxial nanowire is shown in Figure S4. Corresponding energy-dispersive X-ray (EDX) elemental mapping showed the presence of three elements (C, Cu, and O) in the GDY/CuO coaxial nanowire, which is consistent with the X-ray photoelectron spectroscopy (XPS) result (Figure 2e), indicating that GDY shells were successfully coated on the surface of the CuO nanowires. The growth of GDY could be further evidenced by the Raman spectrum shown in Figure 2d, where the peak at 2178.9 cm^{-1} can be assigned to the vibration of conjugated diyne links, indicating a successful coupling reaction.[27,28] The C 1s peak in Figure 2e can be deconvoluted into four subpeaks at 284.5, 285.1, 286.3, and 288.0 eV, corresponding to C—C (sp^2), C—C (sp), C—O, and C═O, respectively (Figure 2f). The area ratio of the sp- and sp^2-hybridized carbon atoms was about 2, consistent with the model structure of graphdiyne in which the benzene rings link with each other by the conjugated diyne links in GDY.[29]

As mentioned above, GDY/CuO coaxial nanowires with uniformity and porous microstructures have been formed on the surface of a copper foam. With a narrow band gap (0.46 eV) of GDY and uniformly porous microstructures, GDY-based nanowires are expected to exhibit superior optical absorption properties. As schematically shown in Figure 3a, the ray of light

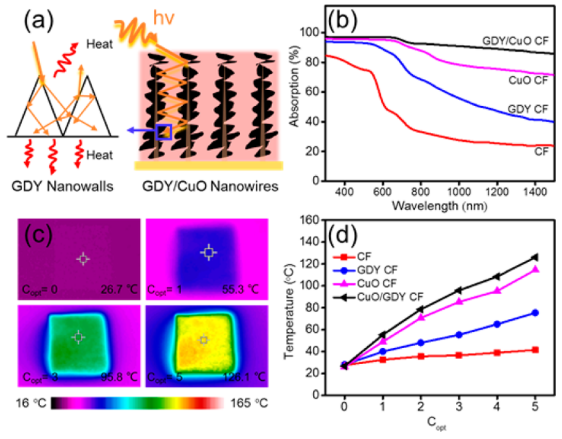

Figure 3. (a) Schematic illustration of the multiple reflection effect. (b) Absorption spectra of commercial copper foam (CF), copper foam with a film of GDY nanowalls on the surface (denoted as GDY CF), copper foam with a film of CuO nanowires (denoted as CuO CF), and copper foam with a film of GDY/CuO coaxial nanowires (denoted as GDY/CuO CF). (c) Infrared (IR) images of GDY/CuO CF under 1 kW m^{-2} (C_{opt}= 1), 3 kW m^{-2} (C_{opt}= 3), and 5 kW m^{-2} (C_{opt}= 5) irradiation from a solar simulator. (e) Plot of irradiation density and sample temperature under different solar irradiations (irradiation density denoted as C_{opt}).

shined on the surface could be reflected and refracted for many times, and is eventually absorbed by the hierarchical structure. The multiple interaction between light and the materials greatly improves the utilization of the solar irradiation.

The optical absorption properties of as-prepared GDY-based structures were carefully examined by optical diffuse reflection, transmittance, and absorption spectra, respectively, shown in Figure 3b and Figure S5. The GDY-based hierarchical nanowires coated copper foam (GDY/CuO CF) shows an average absorption of 92% in the visible to near-IR range and 86% over the whole range of the solar spectrum. The absorbed energy density over the whole solar spectrum is also shown in Figure S6, from which the absorption of solar energy by the samples was calculated (more details in SI). The GDY/CuO CF can achieve 94% energy absorption under 1 kW m^{-2} illumination. This is in contrast with blank copper foam substrate which showed a high reflectance (~60%) and

DOI: 10.1021/acs.chemmater.7b01838
Chem. Mater. 2017, 29, 5777−5781

transmittance (~5%), with the energy density absorption of only 47%. Moreover, the GDY-based nanowires arrays showed low reflective losses compared to GDY nanowalls film (SEM images shown in Figure S7).

To show that the vertical GDY nanosheets played a critical role in the high absorption of energy density, the GDY/CuO nanowires arrays were replaced by single component CuO nanowires arrays (SEM images shown in Figure S8). The CuO CF showed a lower average absorption of 84% in the visible to near-IR range and 75% over the whole range of the solar spectrum (Figure 3b and Figure S6). The absorded energy density over the whole solar spectrum was also calaulated. The CuO CF can only achieve 86% energy absorption (Figure S6), 8% less than that of GDY/CuO CF. Photothermal conversion performance was investigated by the temperature elevation of the as-prepared samples under solar irradiation. The temperature increase and thermal images were characterized by an infrared (IR) camera (Figure 3c and Figure S9). Upon the same irradiation density (5 kW m^{-2}), the temperature of the GDY/CuO CF rose sharply and reached an equilibrium temperature of about 126 °C, indicating great photothermal performance. In the absence of the GDY layer, the CuO nanowires substrate showed a lower equilibrium temperature of 108 °C under irradiation due to the less light harvest efficiency. For comparison, the equilibrium temperature of the undecorated copper foam (41 °C) is also shown in Figure 3d.

The outstanding light absorption of GDY-based nanowires foam offers unique opportunity for the development of highly efficient solar steam generation systems. A GDY-based solar-driven water steam evaporation system was demonstrated by using a solar simulator and a GDY/CuO CF floating on the top of water in a quartz beaker (Figure 4a). The GDY/CuO CF

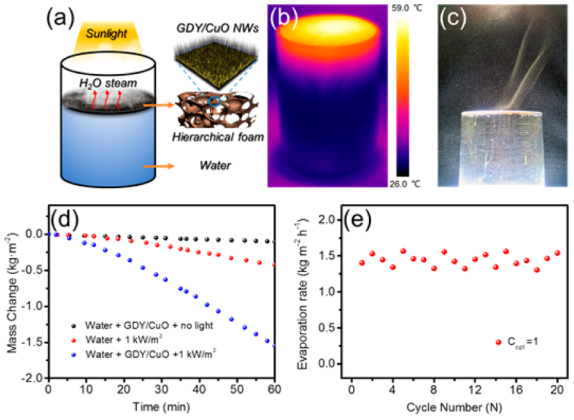

Figure 4. (a) Schematic illustration of the solar steam generation experiment. (b) IR image of GDY/CuO CF on the top of the water surface under the solar illumination of 5 kW m^{-2} for 10 min. (c) Optical image of enhanced steam generation by the GDY/CuO CF under the solar illumination of 8 kW m^{-2}. (d) Plot of the weight loss through water evaporation under solar illumination as a function of irradiation time. (e) Evaporation cycle performance of the GDY/CuO CF.

floated on the water because of its hydrophobicity (Figure S10), with a static contact angle of 137° on the surface of water. Under illumination, GDY and CuO absorbed light and converted it to the thermal energy, which conducted via the copper skeleton and quickly distributed throughout the whole foam. The water was directly heated at the interface between the material and water surface, accelerating the process of evaporation and offsetting the heat loss due to thermal exchange with bulk water.

A picture of the system is shown in Figure S11, where the GDY/CuO nanowires foam with a diameter of 45 mm and a thickness of 1 mm floated on the surface of water. The heat localization of GDY/CuO CF was investigated by corresponding IR images (Figure 4b), which can improve the solar vapor generation by preventing energy losses during the heating process of bulk water. Under the solar illumination of 5 kW m^{-2} for 10 min, the temperature at the surface of water increased to about 59 °C while that at the bottom was about 30 °C (Figure S12), with a temperature difference of 29 °C. In contrast, under the identical solar illumination, the temperature difference in the unit without GDY/CuO CF was less than 3 °C, showing a negligible rise in temperature (Figure S13). These results confirmed that the hot zones were strongly localized on the surface of water with the floating GDY-based foam, accelerating the water evaporation. Figure 4c shows the picture of water evaporation under 8 kW m^{-2} solar illumination. A movie of the solar steam generation by heat localization is shown in the SI. This structure shows great potential for desalination and water purification using sunlight as the only energy source by collecting the condensed water from the steam.

The performance of solar vapor generation of our samples was monitored by the weight loss of water during the evaporation process. As expected, GDY/CuO CF induced the highest evaporation efficiency under the solar illumination of 1 kW m^{-2} among various as-prepared samples (Figure S14). We observed an evaporation rate of 1.55 kg m^{-2} h^{-1} for GDY/CuO CF at 1 kW m^{-2} solar illumination, which was 3.69 times higher than pure water evaporation (Figure 4d). The GDY-based foam presented stable performance during 20 evaporation cycles (Figure 4e), and the morphology after solar irradiation was characterized by SEM (Figure S15), indicating the good stability. The water evaporation rate with free-floating CDY/CuO CF in a dark environment was 0.10 kg m^{-2} h^{-1}, which was subtracted from all the measured evaporation rates under the solar illumination.

To study further the solar vapor generation performance of the GDY-based nanowires foam, the photothermal efficiency (η) of as-prepared foam was estimated using the following equation:[30]

$$\eta = \frac{m\Delta H}{Q} \quad (1)$$

where η is the photothermal efficiency, m is the mass flux of evaporated water, and ΔH is the total enthalpy of liquid−vapor phase change. Q is the solar illumination density on the samples. The efficiency of GDY/CuO CF can achieve 91% at power density of 1 kW m^{-2}, higher than most of previous reports[8,9,22,30−32] under 1 kW m^{-2} illumination (Figure S16). The efficiencies of the controls (CuO CF, GDY CF, and CF) are shown in Figure S17 for comparison. Because of the minimized surface reflection and the promoted multiple absorption of light and the large specific surface area for heat exchange, GDY/CuO CF showed the highest efficiency. Moreover, the photothermal efficiency of GDY/CuO CF was also investigated under various solar illumination conditions (Figure S18, 19).

In conclusion, we reported a GDY-based free-floating foam with a multidimensional architecture, which exhibited highly efficient solar steam generation. GDY/CuO coaxial nanowires

DOI: 10.1021/acs.chemmater.7b01838
Chem. Mater. 2017, 29, 5777−5781

were obtained on the robust copper foam via a low-cost and scalable solution process. Such a structure showed excellent solar energy absorption over the whole solar spectrum, and possessed porous networks for efficient vapor flow. The GDY/CuO CF can achieve 91% photothermal efficiency under 1 kW m^{-2} illumination. With the cost-effective solution process and high photothermal efficiency, this type of GDY-based solar steam generation promises a wide range of applications such as desalination and related technologies.

■ ASSOCIATED CONTENT

Supporting Information

The Supporting Information is available free of charge on the ACS Publications website at DOI: 10.1021/acs.chemmater.7b01838.

Experimental details, characterization methods, supplementary figures (PDF)

Solar steam generation video (AVI)

■ AUTHOR INFORMATION

Corresponding Authors

*J. Zhang. E-mail: jinzhang@pku.edu.cn.

*Z. Liu. E-mail: zfliu@pku.edu.cn.

*L. Tong. E-mail: tonglm@pku.edu.cn.

ORCID

Hailin Peng: 0000-0003-1569-0238

Zhongfan Liu: 0000-0003-0065-7988

Jin Zhang: 0000-0003-3731-8859

Author Contributions

§These authors contributed equally to this work.

Notes

The authors declare no competing financial interest.

■ ACKNOWLEDGMENTS

This work was supported by the Ministry of Science and Technology of China (2016YFA0200101 and 2016YFA0200104) and the National Natural Science Foundation of China (grants 51432002, 21129001, 21233001).

■ REFERENCES

(1) Karagiannis, I. C.; Soldatos, P. G. Water desalination cost literature: review and assessment. *Desalination* **2008**, *223*, 448−456.

(2) Zhou, L.; Tan, Y.; Wang, J.; Xu, W.; Yuan, Y.; Cai, W.; Zhu, S.; Zhu, J. 3D self-assembly of aluminium nanoparticles for plasmon-enhanced solar desalination. *Nat. Photonics* **2016**, *10*, 393−398.

(3) Sharon, H.; Reddy, K. S. A review of solar energy driven desalination technologies. *Renewable Sustainable Energy Rev.* **2015**, *41*, 1080−1118.

(4) Shannon, M. A.; Bohn, P. W.; Elimelech, M.; Georgiadis, J. G.; Marinas, B. J.; Mayes, A. M. Science and technology for water purification in the coming decades. *Nature* **2008**, *452*, 301−310.

(5) Gupta, M. K.; Kaushik, S. C. Exergy analysis and investigation for various feed water heaters of direct steam generation solar-thermal power plant. *Renewable Energy* **2010**, *35*, 1228−1235.

(6) Wang, J.; Li, Y.; Deng, L.; Wei, N.; Weng, Y.; Dong, S.; Qi, D.; Qiu, J.; Chen, X.; Wu, T. High-Performance Photothermal Conversion of Narrow-Bandgap Ti2O3 Nanoparticles. *Adv. Mater.* **2017**, *29*, 1603730.

(7) Wang, Z.; Liu, Y.; Tao, P.; Shen, Q.; Yi, N.; Zhang, F.; Liu, Q.; Song, C.; Zhang, D.; Shang, W.; Deng, T. Bio-Inspired Evaporation Through Plasmonic Film of Nanoparticles at the Air-Water Interface. *Small* **2014**, *10*, 3234−3239.

(8) Ghasemi, H.; Ni, G.; Marconnet, A. M.; Loomis, J.; Yerci, S.; Miljkovic, N.; Chen, G. Solar steam generation by heat localization. *Nat. Commun.* **2014**, *5*, 4449.

(9) Hu, X.; Xu, W.; Zhou, L.; Tan, Y.; Wang, Y.; Zhu, S.; Zhu, J. Tailoring Graphene Oxide-Based Aerogels for Efficient Solar Steam Generation under One Sun. *Adv. Mater.* **2017**, *29*, 1604031.

(10) Jiang, Q.; Tian, L.; Liu, K.-K.; Tadepalli, S.; Raliya, R.; Biswas, P.; Naik, R. R.; Singamaneni, S. Bilayered Biofoam for Highly Efficient Solar Steam Generation. *Adv. Mater.* **2016**, *28*, 9400−9407.

(11) Li, X.; Xu, W.; Tang, M.; Zhou, L.; Zhu, B.; Zhu, S.; Zhu, J. Graphene oxide-based efficient and scalable solar desalination under one sun with a confined 2D water path. *Proc. Natl. Acad. Sci. U. S. A.* **2016**, *113*, 13953−13958.

(12) Li, Y.; Xu, L.; Liu, H.; Li, Y. Graphdiyne and graphyne: from theoretical predictions to practical construction. *Chem. Soc. Rev.* **2014**, *43*, 2572−2586.

(13) Zhang, S.; Du, H.; He, J.; Huang, C.; Liu, H.; Cui, G.; Li, Y. Nitrogen-Doped Graphdiyne Applied for Lithium-Ion Storage. *ACS Appl. Mater. Interfaces* **2016**, *8*, 8467−8473.

(14) Zhang, S.; Liu, H.; Huang, C.; Cui, G.; Li, Y. Bulk graphdiyne powder applied for highly efficient lithium storage. *Chem. Commun.* **2015**, *51*, 1834−1837.

(15) Jin, Z.; Yuan, M.; Li, H.; Yang, H.; Zhou, Q.; Liu, H.; Lan, X.; Liu, M.; Wang, J.; Sargent, E. H.; Li, Y. Graphdiyne: An Efficient Hole Transporter for Stable High-Performance Colloidal Quantum Dot Solar Cells. *Adv. Funct. Mater.* **2016**, *26*, 5284−5289.

(16) Li, J.; Gao, X.; Liu, B.; Feng, Q.; Li, X.-B.; Huang, M.-Y.; Liu, Z.; Zhang, J.; Tung, C.-H.; Wu, L.-Z. Graphdiyne: A Metal-Free Material as Hole Transfer Layer To Fabricate Quantum Dot-Sensitized Photocathodes for Hydrogen Production. *J. Am. Chem. Soc.* **2016**, *138*, 3954−3957.

(17) Gao, X.; Li, J.; Du, R.; Zhou, J.; Huang, M. Y.; Liu, R.; Li, J.; Xie, Z.; Wu, L. Z.; Liu, Z.; Zhang, J. Direct Synthesis of Graphdiyne Nanowalls on Arbitrary Substrates and Its Application for Photoelectrochemical Water Splitting Cell. *Adv. Mater.* **2017**, *29*, 1605308.

(18) Wang, S.; Yi, L.; Halpert, J. E.; Lai, X.; Liu, Y.; Cao, H.; Yu, R.; Wang, D.; Li, Y. A novel and highly efficient photocatalyst based on P25-graphdiyne nanocomposite. *Small* **2012**, *8*, 265−271.

(19) Qi, H.; Yu, P.; Wang, Y.; Han, G.; Liu, H.; Yi, Y.; Li, Y.; Mao, L. Graphdiyne oxides as excellent substrate for electroless deposition of pd clusters with high catalytic activity. *J. Am. Chem. Soc.* **2015**, *137*, 5260−5263.

(20) Gao, X.; Zhou, J.; Du, R.; Xie, Z.; Deng, S.; Liu, R.; Liu, Z.; Zhang, J. Robust Superhydrophobic Foam: A Graphdiyne-Based Hierarchical Architecture for Oil/Water Separation. *Adv. Mater.* **2016**, *28*, 168−173.

(21) Long, M.; Tang, L.; Wang, D.; Li, Y.; Shuai, Z. Electronic Structure and Carrier Mobility in Graphdiyne Sheet and Nanoribbons: Theoretical Predictions. *ACS Nano* **2011**, *5*, 2593−2600.

(22) Ito, Y.; Tanabe, Y.; Han, J.; Fujita, T.; Tanigaki, K.; Chen, M. Multifunctional Porous Graphene for High-Efficiency Steam Generation by Heat Localization. *Adv. Mater.* **2015**, *27*, 4302−4307.

(23) Zhang, W.; Wen, X.; Yang, S.; Berta, Y.; Wang, Z. L. Single-Crystalline Scroll-Type Nanotube Arrays of Copper Hydroxide Synthesized at Room Temperature. *Adv. Mater.* **2003**, *15*, 822−825.

(24) Zhou, J.; Gao, X.; Liu, R.; Xie, Z.; Yang, J.; Zhang, S.; Zhang, G.; Liu, H.; Li, Y.; Zhang, J.; Liu, Z. Synthesis of Graphdiyne Nanowalls Using Acetylenic Coupling Reaction. *J. Am. Chem. Soc.* **2015**, *137*, 7596−7599.

(25) Yang, W.; Wang, J.; Ma, W.; Dong, C.; Cheng, G.; Zhang, Z. Free-standing CuO nanoflake arrays coated Cu foam for advanced lithium ion battery anodes. *J. Power Sources* **2016**, *333*, 88−98.

(26) Wu, F.; Banerjee, S.; Li, H.; Myung, Y.; Banerjee, P. Indirect Phase Transformation of CuO to Cu_2O on a Nanowire Surface. *Langmuir* **2016**, *32*, 4485−4493.

(27) Li, G.; Li, Y.; Liu, H.; Guo, Y.; Li, Y.; Zhu, D. Architecture of graphdiyne nanoscale films. *Chem. Commun.* **2010**, *46*, 3256−3258.

DOI: 10.1021/acs.chemmater.7b01838
Chem. Mater. 2017, 29, 5777−5781

(28) Zhang, S.; Wang, J.; Li, Z.; Zhao, R.; Tong, L.; Liu, Z.; Zhang, J.; Liu, Z. Raman Spectra and Corresponding Strain Effects in Graphyne and Graphdiyne. *J. Phys. Chem. C* **2016**, *120*, 10605−10613.
(29) Haley, M. M.; Brand, S. C.; Pak, J. J. Carbon networks based on dehydrobenzoannulenes: synthesis of graphdiyne substructures. *Angew. Chem., Int. Ed. Engl.* **1997**, *36*, 836−838.
(30) Wang, Y.; Zhang, L.; Wang, P. Self-Floating Carbon Nanotube Membrane on Macroporous Silica Substrate for Highly Efficient Solar-Driven Interfacial Water Evaporation. *ACS Sustainable Chem. Eng.* **2016**, *4*, 1223−1230.
(31) Wang, X.; Ou, G.; Wang, N.; Wu, H. Graphene-based Recyclable Photo-Absorbers for High-Efficiency Seawater Desalination. *ACS Appl. Mater. Interfaces* **2016**, *8*, 9194−9199.
(32) Hua, Z.; Li, B.; Li, L.; Yin, X.; Chen, K.; Wang, W. Designing a Novel Photothermal Material of Hierarchical Microstructured Copper Phosphate for Solar Evaporation Enhancement. *J. Phys. Chem. C* **2017**, *121*, 60−69.

DOI: 10.1021/acs.chemmater.7b01838
Chem. Mater. 2017, 29, 5777−5781